

Electrokinetic micropump and micromixer design based on ac faradaic polarization

Dmitri Lastochkin, Ronghui Zhou, Ping Wang, Yuxing Ben, and Hsueh-Chia Chang

Center for Micro-fluidics and Medical Diagnostics, Department of Chemical and Biomolecular Engineering, University of Notre Dame, Notre Dame, Indiana 46556

(Received 1 March 2004; accepted 10 May 2004)

A microfluidic pump and mixer design based on ac faradaic polarization is proposed. Unlike ac electrokinetic devices based on capacitive charging of the electrodes, the design yields a net electro-osmotic flow for high-conductivity electrolytes at high voltages and frequencies without producing gas bubbles or generating pH gradients. The average velocity, which can be more than an order of magnitude higher than that generated by the capacitive mechanism, has an exponential dependence on the voltage and increases monotonically at low frequencies. Vortices and net flows with linear velocities in excess of 1 mm/s are generated with orthogonal microfabricated planar electrodes based on the unique flow and polarization features of this new ac charging mechanism. © 2004 American Institute of Physics. [DOI: 10.1063/1.1767286]

I. INTRODUCTION

Because mechanical micropumps with moving parts are prone to frictional wear in microfluidic devices, the use of electrokinetic pumps, which have no moving parts, to transport and mix fluids has attracted considerable attention recently. The simplest of such pumps is a dc pump for electrolytes in which the electro-osmotic flow is sustained by a field E applied between two electrodes at ends of the flow channel.¹ The field produces a tangential Maxwell force within the naturally polarized wall Debye layer (by the surface functional group of the channel wall) and drives a characteristic tangential Smoluchowski surface velocity U_s of the order $\epsilon\xi E/\mu$, where ϵ is the permittivity of the electrolyte, ξ is the zeta potential of the Debye layer that measures the polarization with the layer, and μ the electrolyte viscosity. This zeta potential rarely exceeds 100 mV. With nonuniform zeta potential due either to inhomogeneous functionalization² or by nonuniform dc charging,³ the dc electroosmotic slip velocity can be nonuniform such that vortices are created. Hence, both dc micropumps and dc micromixers can be fabricated by this electrokinetic mechanism.

However, a severe limitation of dc pumps is that the electrode reactions that sustain the dc current tend to generate bubbles and produce significant pH gradients (that sensitively affect the double layer polarization and electrokinetic phenomena) in microchannels and reservoirs.⁴ An ac faradaic pump is proposed in this report to alleviate this shortcoming.

II. AC ELECTRO-OSMOTIC FLOW

More recently, it was realized that ac fields can polarize electrode surfaces and drive a time-averaged net flow on them by a capacitive charging mechanism.^{5–7} If the field frequency is higher than the inverse electrode reaction time, electrode reactions that produce bubbles and pH gradients can be minimized. The ac electrode polarization occurs because the field induces a transient current that charges the Debye layer like a capacitor. The charged layer would par-

tially screen the external field such that the latter develops an outward tangential component on one electrode of a parallel pair that is in the direction away from the other electrode [see Fig. 1(a)].

As the polarization and the tangential field are in phase, the resulting tangential Maxwell force and electro-osmotic flow both point outwards in each half cycle of the applied ac field, thus producing a time-averaged surface velocity in the same direction. The induced Debye layer polarization by the external current produces an effective ζ potential of the order Ed , where d is the electrode separation, at low frequencies when most of the potential drop V across the electrode occurs at the Debye layer. Hence, the characteristic slip velocity U_s now scales as $\epsilon dE^2/\mu$, which is higher than the dc Smoluchowski velocity by a factor of V/ξ . As the reaction time is a sensitive (exponential) function of V , the potential drop is often limited to less than 1V.^{6,8} Nevertheless, even at

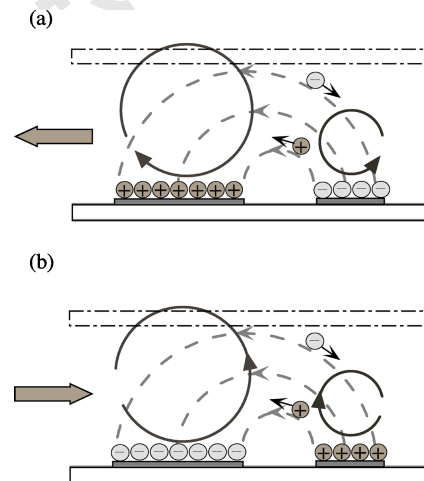


FIG. 1. The electric (dotted curves) and flow (solid curves) fields for asymmetric parallel electrodes by capacitive charging (a) and faradaic charging (b). The fields correspond to the half cycle when the left (larger) electrode is cathode. The upper channel wall is used to produce a net flow in the direction indicated by the large arrow on the left.

this low voltage, the quadratic scaling of ac electrokinetics with respect to E still produces a surface velocity that is more than one order of magnitude higher than the Smoluchowski velocity, as V/ξ is still 10 or larger. Since the external field is completely screened at low frequencies and electrode charging is weak at high frequencies, this surface velocity due to capacitive charging only exists over a frequency range (around 100 kHz for typical electrolytes) near the inverse RC time of the electrode pair, where $R=d/\kappa$ is the resistance of the electrolyte between the electrodes, κ is the conductivity, and C is the Debye layer capacitance per unit area, ϵ/λ . A clear maximum in U_s with respect to the field frequency ω has been observed.^{6,8}

Unlike dc electrokinetics due to natural polarization, the ac electrokinetic surface flow by this capacitive charging mechanism only occurs on electrodes. As such, they will create back flow and vortices at the edges of the electrodes. Even if the entire channel surface is covered with parallel and symmetric electrode pairs, the opposite outward flow on each electrode will drive large vortices without a net flow in one direction. To create a pump with this ac capacitive charging mechanism, asymmetric electrodes are used and a top wall is used to suppress the outer flow of the larger vortex on the larger electrode [see Fig. 1(a)] such that a net flow results.^{5,6}

Micropumps and mixers based on the capacitive charging have operated only at low voltages (<1 V) and at high frequencies (~ 100 kHz) to minimize reaction and to maximize U_s . However, ac faradaic reactions do not necessarily lead to gas formation. Reversible electrode dissolution and deposition reactions, for example, often do not involve gas generation. Even if gas molecules are generated in ac reactions, such as the electrolysis reactions, insignificant amount is generated in each half cycle that the gas molecules can dissolve without nucleating macroscopic bubbles. Negligible net pH generation also may not materialize as ions generated can be consumed by the reverse reaction in the next half cycle. In Fig. 2(a), the voltage-frequency range where macroscopic bubble generation is observed is shown for the two fabricated Al electrode pairs in NaCl on glass in Fig. 3. It is clear that at 100 kHz, the rms voltage must exceed about 14 V, for the given electrolyte, electrode geometry, and material, before macroscopic bubbles are formed. This critical voltage for bubble formation is ten times that for dc currents and it further increases at higher frequency as the reaction time is expected to decrease with voltage exponentially for typical Butler-Volmer-type kinetics.⁹ When bubbles are generated, corrosion on the Al electrodes can be visibly observed at the high voltages shown in Fig. 2(a). In contrast, corrosion is observed only after hours of continual experiments when the voltage is reduced slightly into the no-bubble region. Using pH indicators, we also do not detect significant permanent pH changes near the electrodes at these high voltages.

III. FARADAIC CHARGING

Nevertheless, ac faradaic reaction still occurs¹⁰ and ions are being generated periodically in time at the electrodes

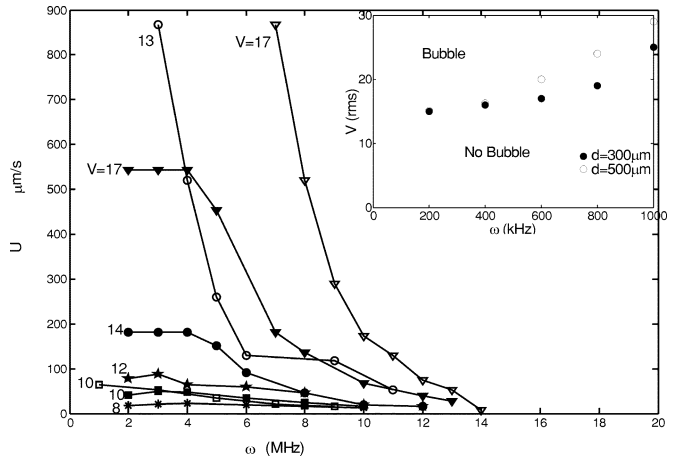


FIG. 2. (a) The critical voltage for bubble generation at a given frequency for both disjointed and continuous Al contiguous T electrodes in NaCl solution with conductivity of $0.001 \text{ S}/\mu\text{m}$. The electrode width is $100 \mu\text{m}$ and the separations are 300 and $500 \mu\text{m}$. (b) The average particle velocity as a function of frequency for the chromel and Pt contiguous T electrodes with $d=150 \mu\text{m}$ and $\kappa=0.1 \text{ S}/\mu\text{m}$ for the indicated voltages. Solid symbols are chromel electrodes and open ones Pt.

even if bubbles are not produced. This ac polarization mechanism due to time-periodic Faradaic reaction is qualitatively distinct from the ac capacitive charging mechanism. Cations are produced at the electrode by the reaction instead of the counterions that move from the bulk by electromigration. As a result, as shown in Fig. 1(b), faradaic polarization has an opposite sign from capacitive charging and the net flow on one electrode is now towards the other electrode.⁵

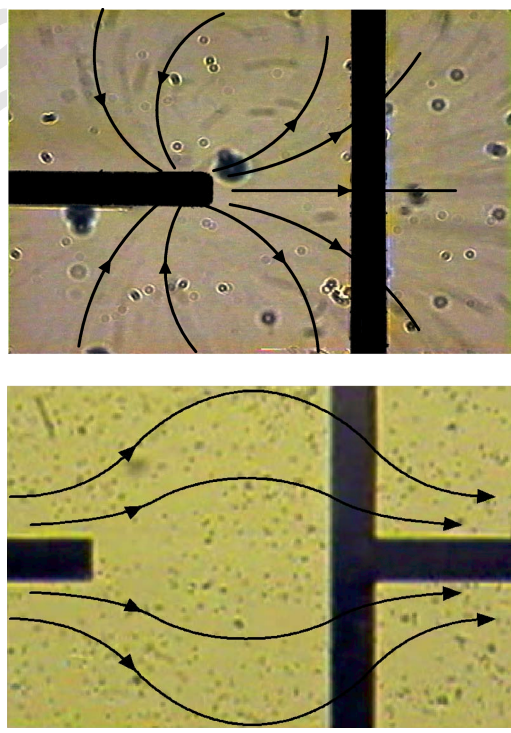


FIG. 3. Planar orthogonal Al electrodes fabricated on glass. Two T-electrode configurations are studied—the top disjointed T and the bottom contiguous T electrodes. The contiguous T electrode is repeated 16 times in a 2 cm long array. The electrodes are $100 \mu\text{m}$ wide, $1000 \mu\text{m}$ long and separated by $d=150\text{--}500 \mu\text{m}$. The trajectories added are from tracking $5 \mu\text{m}$ latex particles, some of which are evident in the top image.

Moreover, since the ions produced by the reaction has the same polarity as the electrode [see Fig. 1(b)], faradaic charging amplifies the external field instead of screening it.

This faradaic charging should also drive an ac electrokinetic velocity on the electrodes but in the direction opposite from the capacitive charging. Due to the lack of screening, the velocity by faradaic charging is expected to increase monotonically or approach a constant asymptote at low frequency. The latter scenario occurs if the reaction is reversible and reaches equilibrium within a half cycle at low frequency. Both scenarios are distinct from that for capacitive charging where an optimum frequency exists.^{5–7} We have indeed observed strong ac electrokinetic surface velocity on ac electrodes for three electrode materials (Al, Pt, and Chromel—an alloy of chrome and nickel), the two T electrode configurations shown in Fig. 3, and a large range of electrolyte composition that is consistent with the new faradaic charging mechanism. The velocity visualization and estimate are done with 5 μm latex particles that are roughly 100 μm above the surface. The flow also occurs within a drop without the top wall in Fig. 1. Due to the absence of a top wall, the velocity is observed to be a weak function of the normal direction, in contrast to those shown in Fig. 1. The longitudinal velocity also does not change much along the longitudinal electrode. The average velocity along this electrode is shown in Fig. 2 as a function of frequency. A constant asymptote for chromel electrodes is reached at 4 MHz and a low-frequency blow-up for Pt electrodes occurs below that frequency. The latter exceeds 1 mm/s beyond 14 V and below 1 MHz. Velocity on Al electrodes also shows a constant low-frequency asymptote that is only reached below several hundred kHz and is not shown. The noble metal Pt is expected to be the best electrode catalyst for electrolysis reactions whereas an alumina film that suppresses reaction is expected to form on Al due to the oxidation reaction at low frequencies. The dependence of the slip velocity on ω for these two materials shown in Fig. 2(b) is hence consistent with these unique features of faradaic charging. It is quite distinct from that for capacitive charging with a clear maximum at $\omega \sim 100$ kHz.

IV. MICROPUMP DESIGN AND FLOW IMAGING

One can employ the same asymmetric parallel electrode design for capacitive charging to drive a net flow in the opposite direction by faradaic charging, as shown in Fig. 1(b). However, the particular flow direction of faradaic charging mechanism motivates the new two-dimensional asymmetric electrode design of Fig. 3 that does not require the use of top-wall shear to suppress momentum transfer of an opposing surface electrokinetic flow (we do not have a top wall in our experiments). With the two-dimensional disjointed T and contiguous T electrodes in Fig. 3, the flow from the tip of the longitudinal electrode is no longer opposed by flow from the transverse electrode.

Moreover, solution of the Laplace equation for the electric potential in the electroneutral bulk is singular at geometric singularities like corners, tips, and cones. In earlier work,¹¹ we have shown that this geometrically enhanced field near a channel corner can produce intense microjets and

vortices in a dc field. The ac fields used in faradaic charging can likewise be enhanced by sharp tip electrodes or by the orthogonal orientation of the two electrodes in our T design of Fig. 3. This geometric enhancement does not exist for the asymmetric planar electrode design of Fig. 1.

Converging flow along the transverse electrode towards its middle is also expected but, due to reflection symmetry, these two transverse flows should cancel each other. We hence expect a net flow in the direction of the tip and over the “transverse” electrode strip. This flow is indeed observed and the streamlines are shown in Fig. 3. The flow in the tip direction is finally arrested by pressure-driven back flow beyond the transverse electrode, as that region of the surface is not covered by electrodes and does not sustain a surface flow. Continuity then stipulates that the blocked flow must recirculate to produce the intense planar vortex pair shown in Fig. 3(a). Unlike the normal vortices across the small flow channel in Fig. 1(b) due to capacitive charging, these planar vortices are much larger and, as they suffer less viscous dissipation, much more intense.

The pressure-driven back flow responsible for the planar vortices can be removed by simply repeating the electrode pair units in an array. This reasoning motivates the T array design shown in Fig. 3(b). The repeated units ensure that there is sufficient surface electrode coverage and a significant pressure-driven back flow is never realized in the longitudinal direction.

The low-frequency asymptotic velocity data for a range of conductivity with the Al continuous T electrode, after the constant asymptote is reached below 500 kHz, are shown in Fig. 3 in scaled variables. The velocity has an exponential dependence on voltage up to 25 V with little sensitivity to electrolyte conductivity. It is also inversely proportional to the electrode separation d . This scaling for U_s is distinctly different from the $\epsilon d E^2 / \mu$ scaling of capacitive charging. It is, however, consistent with faradaic charging as we expect its effective ζ potential to be independent of the external field as the charges are generated by reaction. It is reasonable to assume that the faradaic reaction is an Arrhenius exponential function of the potential drop across the Stern layer. This is consistent with empirical measurements for dc reactions but it is currently impossible to discern whether the relevant potential drop is across the Stern layer or the entire double layer. Nevertheless, one expects an exponential dependence of the effective ζ potential on V , which can be written as $V_0 e^{V/V_0}$ where V_0 is a characteristic voltage. Hence, we expect the faradaic scaling for the velocity to be $U_s \sim e^{V/V_0} \epsilon E V_0 / \mu$ where $E = V/d$. The characteristic voltage V_0 is estimated to be 6.8 V from Fig. 4. Hence, for V larger than 5 V, our fitted slip velocity for Al, $U_s = 1.4 \times 10^{-4} e^{V/V_0} \epsilon E V_0 / \mu$, is a factor of 1.4 $\times 10^{-4} (V/\xi) e^{V/V_0}$ larger than the dc Smoluchowski velocity and a factor of $1.4 \times 10^{-4} e^{V/V_0}$ over the time-average slip velocity of ac capacitive charging. The characteristic voltage V_0 is much lower for Pt (< 1 V) and this scaling represents a significant enhancement at high voltages.

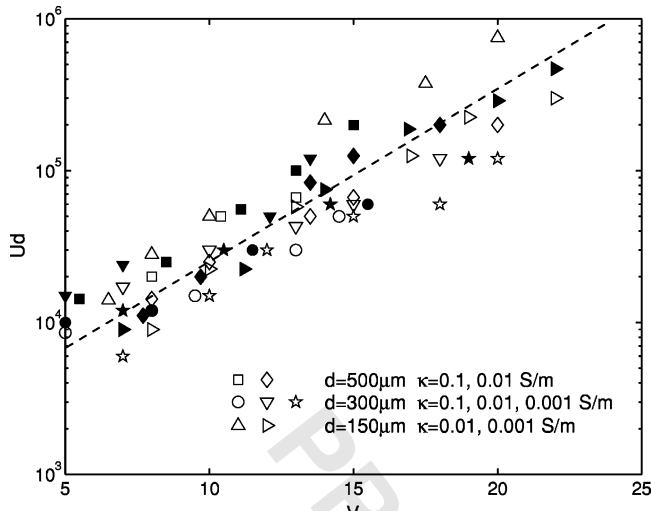


FIG. 4. Collapsed low-frequency asymptotic velocity data for Al electrodes with $d=150, 300, 500 \mu\text{m}$ in NaCl solutions. These electrode separation and electrolyte composition over three orders of magnitude are represented. The solid symbols are for $\omega=200 \text{ kHz}$ and the open ones for $\omega=400 \text{ kHz}$. The fitted curve is $U_s=1.4\times 10^{-4} e^{V/V_0} \epsilon V_0 / \mu$.

V. CONCLUSION

We use transient ac oxidation and reduction reactions to polarize an electrode pair. The high-frequency ($>100 \text{ KHz}$) ac field allows us to elevate V ten times beyond the critical dc voltage for bubble generation. An orthogonal electrode configuration is then used to break the counter-flow geometry to produce a net flow. Since the reaction and polarization rates are exponential functions of the rms voltage V across the double layer, our pump functions well for high-conductivity electrolytes whose overall potential drop V is mostly across the double layer with little drop across the conducting bulk (see Fig. 4). This is in direct contrast to capacitive pumps and dc pumps whose velocity decreases with conductivity. Moreover, the effective ζ potential scales exponentially with respect to V for faradaic charging instead of the linear scaling for capacitive charging.

With exponential scaling with respect to V , the velocity

at 20 V, right below the critical voltage for macroscopic bubble generation, is ten times that at 14 V for faradaic charging for the particular electrode pair at low frequencies. This exemplifies the difference in voltage scaling between faradaic charging and capacitive charging and allows us to reach velocities in excess of mm/s. For a 2 cm array with 16 elements, the power consumption at 20 V is estimated to be less than 0.1 mW, which is high for inefficient electrokinetic pumps. We expect this power input to produce a flow rate of several cubic centimeter per day, which is adequate for drug delivery and liquid fuel cell applications.

ACKNOWLEDGMENTS

P.W. and H.-C.C. were partially supported by the U.S. Army CECOM RDEC through Grant No. DAAB 07-03-3-K414. Such support does not constitute endorsement by the U.S. Army of the views expressed in this publication. D.L. was supported by the Center for Microfluidics and Medical Diagnostics at Notre Dame. R.Z. and H.-C.C. were partially supported on a NASA Grant No. NAG5-10503. Y. B. was supported by the Center for Applied Math at Notre Dame.

- ¹S. Zeng, C. -H. Chen, J. C. Mikkelsen, and J. G. Santiago, *Sens. Actuators B* **79**, 107 (2001).
- ²A. D. Stroock, M. Weck, D. T. Chiu, W. T. S. Huck, P. J. A. Kenis, R. F. Ismagilov, and G. M. Whitesides, *Phys. Rev. Lett.* **84**, 3314 (2000).
- ³Y. Ben and H.-C. Chang, *J. Fluid Mech.* **461**, 229 (2002); S.-C. Wang, Y. W. Lai, Y. Ben and H. -C. Chang, *Ind. Eng. Chem. Res.* (to be published).
- ⁴A. Minerick, A. Ostafin, and H.-C. Chang, *J. Capillary Electrophor.* **23**, 2165 (2002).
- ⁵A. Ajdari, *Phys. Rev. E* **61**, R45 (2000).
- ⁶A. B. D. Brown, C. G. Smith, and A. R. Rennie, *Phys. Rev. E* **63**, 016305 (2000).
- ⁷A. Ramos, H. Morgan, N. G. Green, and A. Castellanos, *J. Phys. D* **31**, 2338 (1998); A. Gonzalez, A. Ramos, N. G. Green, A. Castellanos, and H. Morgan, *Phys. Rev. E* **61**, 4019 (2000); A. Ramos, A. Gonzalez, N. G. Green, and H. Morgan, *ibid.* **67**, 056302 (2003).
- ⁸P. J. Sides, *Langmuir* **17**, 5791 (2001); M. Traw, D. A. Saville, and I. A. Aksay, *ibid.* **13**, 6375 (1997).
- ⁹T. M. Squires and M. Z. Bazant, *Phys. Rev. Lett.* **92**, 066101 (2004).
- ¹⁰A. J. Bard and L. R. Faulkner, *Electrochemical Methods*, (Wiley, New York, 2001).
- ¹¹S. Thamida and H.-C. Chang, *Phys. Fluids* **14**, 4315 (2002); P. Takhistov, K. Duginova, and H.-C. Chang, *J. Colloid Interface Sci.* **263**, 133 (2003).